Optical and electron spin resonance spectroscopy of Ti^{3+}-doped yttrium and gadolinium aluminoborates

1997 J. Phys.: Condens. Matter 9 1649

(http://iopscience.iop.org/0953-8984/9/7/026)

J. Phys.: Condens. Matter **9** (1997) 1649–1660. Printed in the UK PII: S0953-8984(97)77258-8

Optical and electron spin resonance spectroscopy of Ti^{3+}-doped yttrium and gadolinium aluminoborates

G Wang†, H G Gallagher†, T P J Han†, B Henderson†, M Yamaga‡ and T Yosida§

† Department of Physics and Applied Physics, University of Strathclyde, Glasgow G1 1XN, UK
‡ Department of Physics, Gifu University, Yanagido, Gifu 501-11, Japan
§ Nakahihon Automotive College, Sakahogi, Kamo 505, Japan

Received 19 August 1996, in final form 29 October 1996

Abstract. Single crystals of Ti^{3+}-doped aluminoborates $YAl_3(BO_3)_4$ (YAB) and $GdAl_3(BO_3)_4$ (GAB) have been grown by the top-seeded solution growth technique, and the optical absorption, photoluminescence and electron spin resonance (ESR) properties of Ti^{3+} dopants measured at low temperature. The optical absorption spectrum of Ti^{3+} comprises two broad bands with peaks at 514 and 576 nm in YAB and at 520 and 586 nm in GAB. The energy separation of the two bands in each crystal is due to the static Jahn–Teller splitting of the excited ^2E state of the Ti^{3+} ions. Photoluminescence from excited Ti^{3+} ions occurs as a broad band in the near-infrared region with a peak at $\lambda = 747$ nm in YAB and 754 nm in GAB when measured at 14 K. Both absorption and photoluminescence spectra are strongly polarized. The spin Hamiltonian parameters for Ti^{3+} ions substituting at trigonally symmetric Al^{3+} sites in YAB have been determined from the orientation dependence of the ESR spectra. The measured shifts in the components of the g-tensor from the free electron g-value of 2.0023 are interpreted in terms of the mixing of the higher component of the $^2T_2$ ground states and of the ^2E excited state into the lowest $^2T_2$ ground state by spin–orbit interaction.

1. Introduction

The mixed borate compounds $REX_3(BO_3)_4$, where $RE^{3+} = Y^{3+}$ or the lanthanides La^{3+}–Yb^3 and $X^{3+} = Al^{3+}$, Ga^{3+} or Sc^{3+}, are isomorphous with the huntite-structured $CaMg_3(CO_3)_4$, having trigonal crystal structures belonging to the $R32$ space group [1]. Crystals of $YAl_3(BO_3)_4$ (YAB) doped with Nd^{3+} have a dual-function optical capability as non-linear optical and laser gain media [2, 3], with laser operation functioning on narrow spectroscopic lines. In general, broadband tunability of lasers is associated with vibronically broadened optical transitions such as there are in Co^{2+}–MgF_2, Cr^{4+}:YAG, Ti^{3+}–Al_2O_3, Cr^{3+}–$BeAl_2O_4$ and Cr^{3+}–$LiSrAlF_6$. Indeed the many Cr^{3+}-doped gain media, ruby apart, all use the $^4A_2 \leftrightarrow {}^4T_2$ transitions for pump band and laser emission. The first spectroscopic studies of Cr^{3+}:YAB were reported by Blasse and his colleagues [4, 5]. More recently single-pass gain and second-harmonic generation into the UV using Cr^{3+}:YAB and Cr^{3+}:$Y(Ga_{0.5}Al_{0.5})_3(BO_3)_4$ was reported [6]. Studies of Cr^{3+}-doped $REX_3(BO_3)_4$ crystals were extended by the present authors to the growth and optical properties of Cr^{3+}-doped YAB, $YSc_3(BO_3)_4$ (YSB), $GdAl_3(BO_3)_4$ (GAB) and $GdSc_3(BO_3)_4$ (GSB) [7–9]. Here we report the single-crystal growth, optical absorption and fluorescence of the yttrium and gadolinium aluminoborates doped with Ti^{3+} and the ESR spectrum of the Ti^{3+}-doped YAB.

0953-8984/97/071649+12$19.50

2. Experimental details

Early work on Nd:YAB growth showed that a $K_2Mo_3O_{10}$ flux is suitable for growing laser quality crystals although problems with flux inclusions and dopant striations were noted [3, 6]. The present authors reported recently the top-seeded solution growth (TSSG) of Cr^{3+}-doped YAB, GAB, YSB and GSB from modified $K_2Mo_3O_{10}$ fluxes [7–9]. In these cases the problems encountered in growing Nd:YAB were overcome by careful adjustment of the saturation temperature and by adding flux modifiers: 15–20% B_2O_3 or $Li_2B_4O_7$ in the growth of yttrium or gadolinium mixed borates, respectively [7, 8]. These same procedures were followed in growing Ti^{3+}:YAB and Ti^{3+}:GAB. Although there were no growth striations in the Ti^{3+}-doped crystals there was a gradual decrease in Ti^{3+} concentration with growth of the crystal, implying that in YAB and GAB the segregation coefficient of Ti^{3+} exceeds unity. Single crystals were grown with dimensions up to 25 mm × 25 mm × 10 mm shaped as rhombohedral prisms with facets perpendicular to the $a \times b \times c$ crystallographic axes. The growth periods for such crystals were typically ∼6–8 weeks. Spectroscopic studies used samples with approximate dimensions 5 mm × 2 mm × 1 mm cut from the as-grown boule with the short axis parallel to the c-axis of the crystal. The three faces were polished to a high-quality finish on diamond impregnated laps.

The ESR measurements on Ti^{3+}:YAB were made at temperatures in the range 4.2–77 K using a Varian X-band ($\nu \simeq 9.3$ GHz) spectrometer. ESR spectra of Ti^{3+}:GAB are precluded by the excessive absorption of microwave power by Gd^{3+} ($S = 7/2$) ions, which are an intrinsic stoichiometric component of these crystals. The ESR spectrometer employs 270 Hz field modulation and phase sensitive detection. Spectra are recorded as plots of the derivative of the absorbed microwave power as a function of magnetic field. The linewidths, defined as the peak-to-peak separations, Δ_{pp}, of the derivative lines, have been measured at constant microwave power over the temperature range 4–50 K.

The absorption coefficient was measured using a Cary-AVIV double-beam spectrophotometer at 77 and 300 K and wavelengths in the range 200–3500 nm. The polarized optical absorption was measured by placing a Glan–Taylor prism in the sample beam of the spectrophotometer. Luminescence from these samples was excited using an Ar^+ laser or an Ar^+ ion-pumped rhodamine 6G dye laser, the beam propagating parallel to the c-axis of the crystal. The emitted radiation was detected in a 90° orientation relative to excitation at the exit slit of an 0.5 m grating monochromator with a cooled Hamamatsu photo-multiplier tube. Polarized luminescence spectra were measured using a polarizing prism after the sample in the emitted beam. The polarization axis of the prism was rotatable through 2π rad in the plane perpendicular to the direction of the radiation. A half-wave plate then depolarized the radiation in order to minimize effects due to the polarization sensitivity of the grating near 650–700 nm.

3. Experimental results

3.1. ESR measurements

The ESR transitions of Ti^{3+} in YAB are relatively easily saturated at cryogenic temperatures (≃4.2 K) even at low microwave power levels. Figure 1 shows the ESR spectra measured at a microwave power of 0.01 mW and microwave frequency of 9.310 GHz with the magnetic field applied parallel to the c-axis ([0001]) and a-axis ([$\bar{1}2\bar{1}0$]) of the crystal. The ESR spectrum for $B \| c$ is a single resonance line with several weak hyperfine lines due to isotopes ^{47}Ti and ^{49}Ti with nuclear spin $I = 5/2$ and $I = 7/2$ and natural abundance 7.3% and 5.5%,

respectively. The splitting of the Ti^{3+} signal near $B = 4500$ G in figure 1 ($B \| c$) is due to a slight mis-alignment of the crystal axis relative to the magnetic field direction. The weak signal at $B = 4070$ G is due to trace amounts of Cr^{3+} impurities.

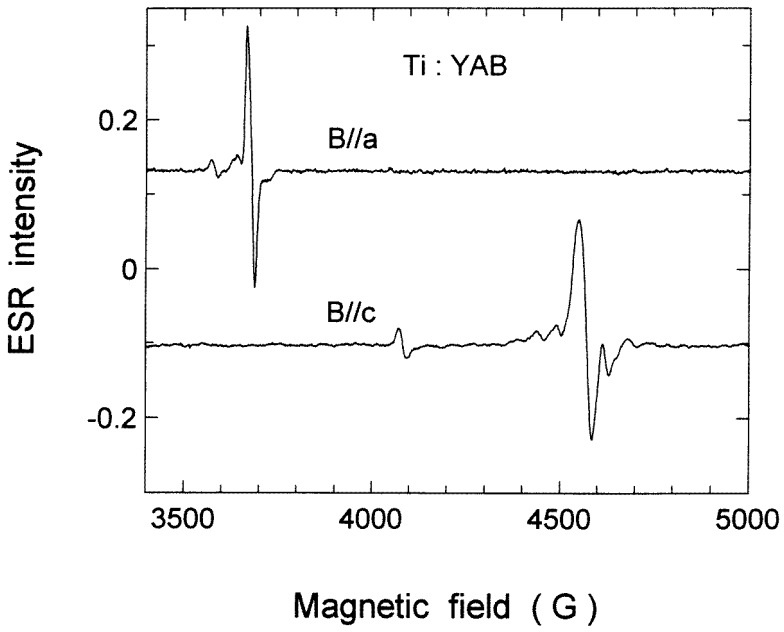

Figure 1. ESR spectra of Ti^{3+}:YAB with magnetic fields applied parallel to the c-axis ([0001]) and a-axis ([$\bar{1}2\bar{1}0$]) observed at 4.2 K.

The angular dependences of the ESR spectra measured for magnetic field rotations in the ($\bar{1}2\bar{1}0$) and (0001) planes are indicated by the open circles at the appropriate resonance fields in figure 2. The ESR spectra at some magnetic field directions consist of three resonance lines, which converge to a single line when the applied magnetic field is parallel to the c-axis. The angular dependences of the ESR spectra are fitted by the spin Hamiltonian:

$$H = g_\xi \mu_B S_\xi B_\xi + g_\eta \mu_B S_\eta B_\eta + g_\zeta \mu_B S_\zeta B_\zeta \tag{1}$$

where S is 1/2, and μ_B is the Bohr magneton. The principal axes ξ, η, and ζ of the g-tensor and the polar angles (θ_ξ, Φ_ξ) for the ξ-axis and $(\theta_\zeta, \Phi_\zeta)$ for the ζ-axis are defined with respect to the abc co-ordinate system in figure 3. The solid curves in figure 2, calculated using (1) with the spin Hamiltonian parameters and the polar angles of the principal axes defined in figure 3 and listed in table 1, are an accurate fit to the angular variations of the ESR signals.

The peak-to-peak intensities of the ESR lines shown in figure 1 decrease rapidly with increasing temperature such that they are not detected above 46 K as a consequence of line broadening induced by spin–lattice relaxation. Figure 4 shows the temperature dependence of the linewidth Δ_{pp} of the ESR lines for measurements with $B \| [\bar{1}2\bar{1}0]$. Note that the linewidth increases abruptly above $T = 35$ K.

Table 1. Spin Hamiltonian parameters and polar angles of principal axis directions of Ti^{3+} ions in YAB.

Crystal	g_ξ	g_η	g_ζ	θ_ξ	ϕ_ξ	θ_ζ	ϕ_ζ
Ti^{3+}:YAB	1.860(5)	1.795(5)	1.445(5)	97(2)	0(2)	7(2)	0(2)

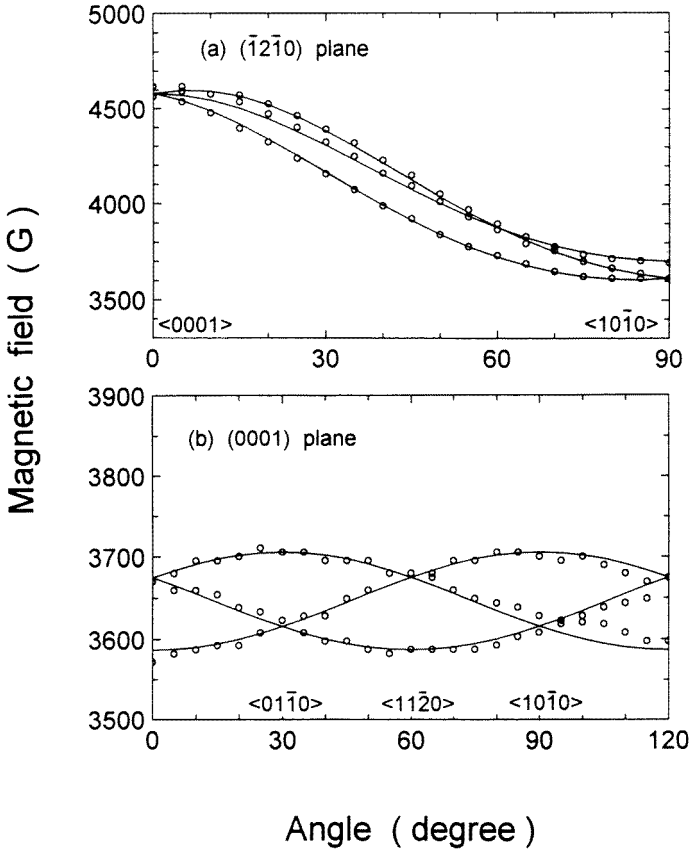

Figure 2. The orientation dependence of the ESR spectrum of Ti^{3+}:YAB at 4.2 K with the magnetic field in (a) the $(\bar{1}2\bar{1}0)$ plane and (b) the (0001) plane. Solid curves are calculated using (1) using the spin Hamiltonian parameters in table 1.

3.2. Polarized optical absorption and photoluminescence

The optical absorption spectra of Ti^{3+} in YAB and GAB measured at 300 K are shown in figure 5 to reveal two overlapping absorption bands with peaks at 514 and 576 nm in YAB and 520 and 586 nm in GAB. In contrast, the photoluminescence spectra in figure 6 show a single broad band in each crystal with peaks at 747 nm in YAB and 755 nm in GAB at $T = 14$ K: these bands shift to longer wavelengths at higher temperatures, the shifts amounting to $\sim$10 nm between 14 and 300 K for both crystals. The weak zero-phonon and phonon-assisted lines observed in other Ti^{3+}-doped crystals were not detected in either case. However, the Ti^{3+} broad band emissions are overlapped on the short-wavelength

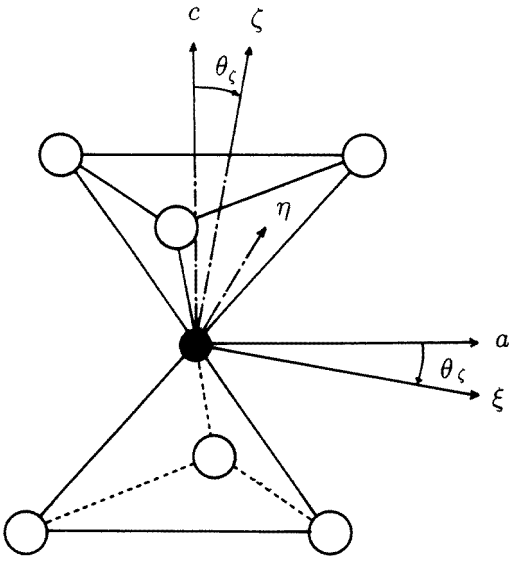

Figure 3. Principal axes ξ, η, and ζ and their polar angles for one of three Ti^{3+} octahedra with respect to the *abc* coordinate system.

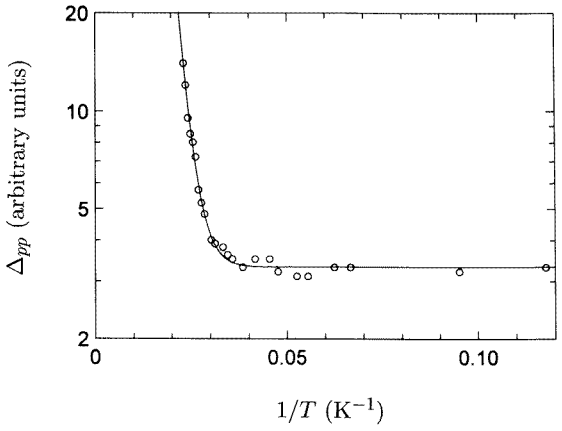

Figure 4. The temperature dependence of the linewidth Δ_{pp} of the ESR spectra of Ti^{3+}:YAB at $B\|[\bar{1}2\bar{1}0]$. The solid curve is calculated using (9) and parameters $a' = 3.3$, $c' = 59\,000$ and $\delta_1 = 258$ cm^{-1}.

edge by the R_1- and R_2-lines of Cr^{3+} ions present in YAB and GAB as trace impurities. The weak vibronic sidebands of the R-lines [8, 9] are hardly detectable at 14 K against the strong photoluminescence band of the Ti^{3+} dopant. Figures 5 and 6, respectively, also show the polarization dependences of the optical absorption and photoluminescence spectra. The absorption bands have π/σ intensity ratios of 3:1 for YAB and 1.5:1 for GAB. Similarly, the π/σ luminescence intensities are 1.4:1 for YAB and 1.4:1 in GAB.

The radiative decay after pulsed excitation is quite fast and follows a single exponential process at low temperature. In YAB the characteristic decay time is 7.9 ± 0.5 μs at $T = 14$ K

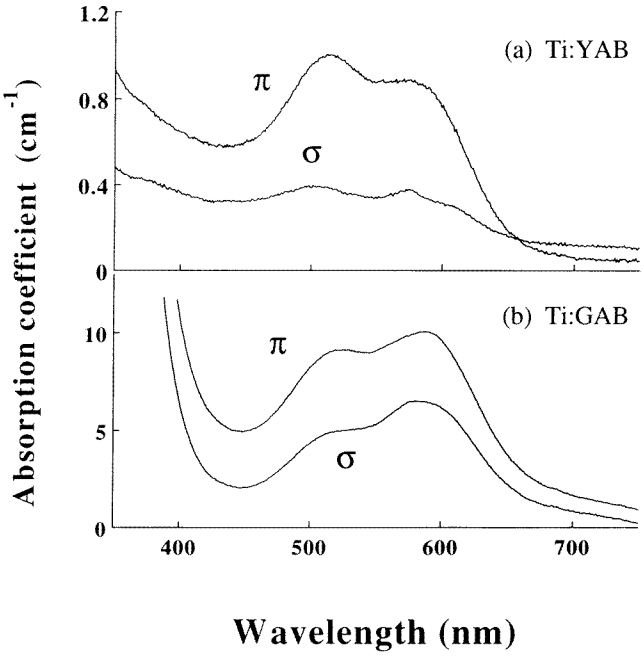

Figure 5. The polarized optical absorption spectra of Ti^{3+} ions in (a) YAB and (b) GAB, measured at 300 K. The polarizations are defined as follows: π-polarization has the E-vector of the radiation parallel to the symmetry axis (in this case the c-axis) and in σ-polarization E is perpendicular to the symmetry axis.

compared with a value of 8.9 ± 0.5 μs in GAB. At 300 K the decay rate is much faster, corresponding to lifetimes of $\sim$1.0 μs. The lifetime of the luminescence decay is again consistent with electric dipole transitions induced by odd-parity distortions of the crystal field. The values of $\tau_R \approx$ 8–9 μs at 14 K are similar to the values reported for other Ti^{3+}-doped crystals. The enhanced excited state decay rate at 300 K results from phonon-induced non-radiative processes [10].

4. Discussion

The Ti^{3+} ion has the $3d^1$ electron configuration outside the closed shells and a resulting ^2D ground state for the free ion. In octahedrally coordinated sites ^2D splits into ^2E and $^2T_2$ states, separated in energy by the octahedral crystal field energy of 10Dq. The Ti^{3+} ion substitutes for Al^{3+} in such crystals as Al_2O_3 and $Y_3Al_5O_{12}$ where the symmetry is distorted by trigonal displacements of the environment. Such distortions in concert with spin–orbit coupling completely remove the fivefold orbital degeneracy of the $3d^1$ configuration [11, 12]. The consequences of these splittings and the strong electron–phonon coupling are the two overlapping absorption bands in the visible region, where the peaks are separated by $\sim$2000–2500 cm^{-1}. Luminescence transitions occur from the lower excited state to the three components of the electronic ground state. If the ground-state splitting is less than the width of the band due to the transition, the luminescence results in a single broad band. Ti^{3+} ions also substitute for Al^{3+} ions in the aluminoborates discussed here: the Al^{3+} sites in these crystals also undergo strong trigonal distortions. Consideration of

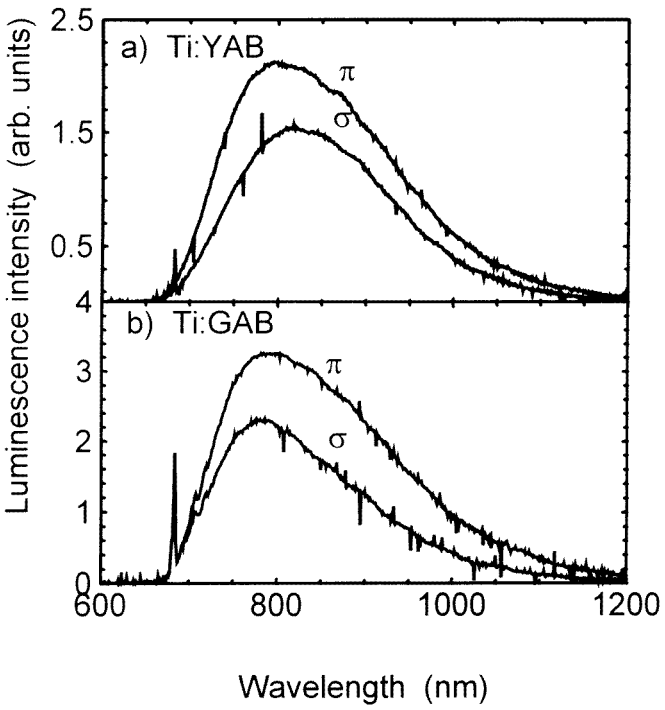

Figure 6. Polarized luminescence spectra of Ti^{3+} ions in the aluminoborate hosts (a) YAB and (b) GAB measured at 14 K. Also revealed are the sharp R-lines near 685 nm due to trace amounts of Cr^{3+} impurity in the crystal.

the ESR and optical spectra reveals the magnitude of the splittings of the ^2E and $^2T_2$ states induced by these distortions.

In octahedral symmetry the wavefunctions of the orbitally degenerate ^2E state are proportional to $|3z^2 - r^2\rangle$ and $|x^2 - y^2\rangle$ whereas those of $^2T_2$ are proportional to $|yz\rangle$, $|xz\rangle$ and $|xy\rangle$. A trigonal distortion of the octahedron leaves ^2E unaffected but mixes together the wavefunctions of $^2T_2$. In trigonal symmetry, the admixed wavefunctions of the $^2T_2$ ground state are represented by

$$|Z\rangle = (1/\sqrt{3})(|xy\rangle + |yz\rangle + |zx\rangle) \qquad ^2A_1 \tag{2}$$

$$\left.\begin{aligned} |X\rangle &= (1/\sqrt{6})(2|xy\rangle - |yz\rangle - |zx\rangle) \\ |Y\rangle &= (1/\sqrt{2})(|yz\rangle - |zx\rangle) \end{aligned}\right\} \quad ^2E. \tag{3, 4}$$

The principal ζ-axis of the Ti^{3+} complex in YAB crystals is determined from the ESR data to be tilted by 7° from the c-axis toward the a-axis. If the tilting angle is assumed to be negligibly small, the degenerate ^2E state in (3) and (4) in trigonal symmetry splits into $|X\rangle$ and $|Y\rangle$, and the energy separation is smaller than that between $^2A_1$ and ^2E of $^2T_2$. On the other hand, the wavefunctions of the ^2E excited state are represented by a linear combination of $|3z^2 - r^2\rangle$ and $|x^2 - y^2\rangle$ orbitals. Such a distorted octahedron is regarded as having pseudo-trigonal symmetry. Figure 7(a) shows the static electronic energy levels of octahedrally coordinated Ti^{3+} ions in the pseudo-trigonal crystal field.

The g-tensor for the pure $|X\rangle$ ground state of Ti^{3+} in pseudo-trigonal symmetry is calculated in terms of mixing of the wavefunctions of the higher-energy components $|Y\rangle$,

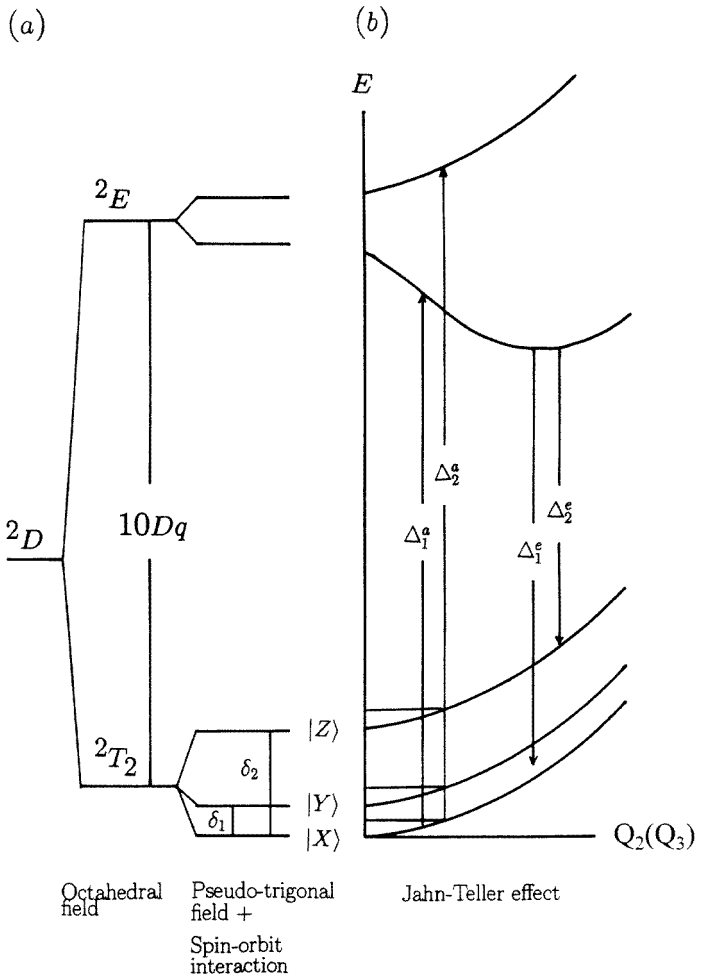

Figure 7. Energy level structure of Ti^{3+} ions in YAB as determined from optical and ESR spectra: (a) a combination of pseudo-trigonal crystal field and spin–orbit interaction and (b) including the Jahn–Teller effect.

$|Z\rangle$, and of the ^{2}E excited state induced by the spin–orbit interaction. The contribution of the ^{2}E excited state to the shift from the g-value of the free electron is much smaller than that of the higher-energy components of $^2T_2$ because the separation ($\Delta_1^a \simeq \Delta_2^a \simeq 20\,000$ cm^{-1}) of the ^{2}E excited state from the ground state is much larger than the splitting of the $^2T_2$ ground state. The energy difference ($\Delta_2^a - \Delta_1^a \simeq 2000$ cm^{-1}) of the ^{2}E excited state in the pseudo-trigonal distortion produces a variation in the g-shift smaller by one order of magnitude than the g-shift obtained from the degenerate ^{2}E excited state. In consequence, three components of the g-tensor of Ti^{3+} in the pseudo-trigonal symmetry are calculated under assumption that $\Delta_1 = \Delta_1^a = \Delta_2^a$ for the ^{2}E excited state and are given by [13–15]

$$g_\xi = 2 - 8\lambda/\Delta_1 - (\lambda^2/2)(1/\delta_1 + 1/\delta_2)^2 \tag{5}$$

$$g_\eta = 2 - 2\lambda/\delta_2 - (\lambda^2/2)(1/\delta_1^2 - 1/\delta_2^2) \tag{6}$$

$$g_\zeta = 2 - 2\lambda/\delta_1 + (\lambda^2/2)(1/\delta_1^2 - 1/\delta_2^2) \tag{7}$$

where λ ($=k\zeta$) is an effective spin–orbit parameter, k is the orbital reduction factor which takes into account the effect of covalency, ζ ($=154$ cm^{-1}) is the one-electron spin–orbit parameter, and δ_1 and δ_2 are the energy separations in the ground state, defined in figure 7. The excited-state energy $\Delta_1 \simeq 18\,000$ cm^{-1} is determined as the average of the peak energies of two absorption bands. The g-shift of g_ζ from the free electron g-value, $g = 2.0023$, is larger than those of g_ξ and g_η because the energy δ_1 is much smaller than the energies Δ_1 and δ_2.

The observed g-values are $g_\xi = 1.860(5)$, $g_\eta = 1.795(5)$ and $g_\zeta = 1.445(5)$ with the principal ζ-axis rotated through 7° away from the c-axis as shown in table 1. Since the g-values are in the order $2 > g_\xi > g_\eta > g_\zeta$, the lowest ground state should be $|X\rangle$, this result being consistent with the crystal structure of YAB, where the octahedron is compressed along the c-axis. The parameters λ/δ_1, λ/δ_2 and λ/Δ_1 in (5)–(7) are determined to be 0.30, 0.085 and 0.0085 by fitting the observed g-values to calculated ones. Then, the effective spin–orbit parameter λ and the reduction factor k are calculated to be $\sim$150 cm^{-1} and $\sim$1, respectively. In the same way, the energy separations of the ground states are $\delta_1 = 450$ cm^{-1} and $\delta_2 = 1750$ cm^{-1}.

The ESR spectra are broadened as the temperature increases and are not detected above 46 K. This effect is caused by the temperature dependence of the spin-lattice relaxation time, T_1, given by

$$1/T_1 = aT + bT^n + c\Delta E^3 \exp[-\Delta E/kT] \tag{8}$$

where ΔE is energy level of the low-lying excited electronic state. The first term in (8) is the direct process. The second and third terms are the Raman and Orbach processes, respectively. At higher temperatures relaxation is dominated by the Orbach process and at lower temperatures by the direct process. The Orbach process is very important for ESR spectra and includes the term of zero-field splitting of the ground state of paramagnetic ions. As the temperature increases, the second component state of the $^2T_2$ ground state of Ti^{3+}, where ΔE is equal to δ_1 in figure 7, is thermally populated. The lifetime of the lowest orbital component of the $^2T_2$ ground state is associated with the spin–lattice relaxation time T_1. Then, the linewidth of the ESR lineshape is proportional to $1/T_1$. Assuming that the Orbach process in (8) is dominant and taking into account the experimental data that the linewidth of Δ_{pp} is nearly constant in the range 0.5–1.0 of $1/T$, the linewidth Δ_{pp} is represented by

$$\Delta_{pp} = a' + c' \exp[-\delta_1/T]. \tag{9}$$

The solid curve in figure 4, calculated using (9) and parameters $a' = 3.3$, $c' = 59\,000$, $\delta_1 = 258$ cm^{-1} fits the observed data. This value for δ_1 is different from that ($\sim$450 cm^{-1}) determined from the g-values. The discrepancy is due to the calculation of the g-values leading to equations (5)–(7) which assume that δ_1, $\delta_2 \gg \lambda, \hbar\omega$ (phonon energy). The experimental value of δ_1 obtained as the activation energy from figure 4 is the more accurate determination. The constant value a' suggests that the inhomogeneous linewidth independent of temperature is much larger than the variation of the linewidth produced by the direct process.

ESR measurements cannot be made on Ti^{3+}:GAB as noted above. Crystallographically GAB and YAB are very similar so the gross energy level structure for Ti^{3+} in the two hosts will differ very little. This is confirmed by the values of Δ_1^a, Δ_2^a and Δ_1^e given in table 2. Of course the g-values are more sensitive to the non-octahedral distortions which result in the ground-state splittings δ_1 and δ_2 and the movement of the magnetic ζ-axis away from the c-axis of the crystal. As we now discuss, any such differences between crystals are reflected in the polarization of the optical spectra.

Table 2. Experimental spectral values and an estimation of 10Dq for Ti^{3+}:$RAl_3(BO_3)_4$ compared with other materials [10].

	YAB	GAB	YAG	Al_2O_3	$YAlO_3$
Δ_1^a (cm^{-1})	17 300	17 100	16 700	18 200	20 400
Δ_2^a (cm^{-1})	19 500	19 200	20 000	20 400	23 500
Δ_1^e (cm^{-1})	13 160	13 070	13 300	13 500	16 400
Dq (cm^{-1})	1840	1815	1835	1930	2195
$\tau_{14\ K}$ (μs)	7.9	8.9	53	3.8	17.5
Halfwidth (cm^{-1}) ($^2E \rightarrow {}^2T_2$)[a]	3850	3470	2240	2290	2590
ΔE_{Stoke} (cm^{-1})	5240	5080	5050	5060	4360

[a] The spectra reported in [10] were measured using a photomultiplier tube, the sensitivity of which decreases beyond 900 nm. In consequence, the quoted half-widths of the luminescence in YAG, $YAlO_3$ and Al_2O_3 are probably underestimated.

The double-peak energies Δ_1^a and Δ_2^a observed in YAB and GAB are compared with similarly measured values for Ti^{3+} in YAG, Al_2O_3 and $YAlO_3$ in table 2 [10]. The average of the energies is approximately equal to the octahedral crystal field splitting 10Dq [10]. As table 2 shows Dq values for YAB and GAB are comparable with that of YAG, but somewhat smaller than in Al_2O_3 and $YAlO_3$. As a consequence the centres of gravity of both absorption and emission processes are shifted to longer wavelength relative to Al_2O_3 and $YAlO_3$. The energy separation, $\Delta_2^a - \Delta_1^a$, which is 2300 and 2100 cm^{-1} for YAB and GAB, respectively, is less than 3300 cm^{-1} for YAG and comparable with 2200 cm^{-1} for Al_2O_3 with the same trigonal symmetry. If the separation is produced by a combination of a static trigonal (pseudo-trigonal) distortion and spin–orbit interaction, it is expected to be less than 1000 cm^{-1} [12]. The large separation and width of the two absorption bands imply that a Jahn–Teller effect acts on the ^2E excited state of Ti^{3+} [10, 16, 17]. This may be analysed in terms of the normal modes of distortion of the octahedron, of which only A_{1g}, E_g and T_{2g} modes contribute significantly to the bandshape and level splittings. In a configurational coordinate model [18], the A_{1g} breathing mode contributes most to the bandwidth, but not to energy splitting. The orbital doublet ^2E_g state of Ti^{3+} in octahedral symmetry couples to the E_g and T_{2g} distortion modes, and the E_g mode is dominant. The Jahn–Teller coupling coefficient of the E_g and T_{2g} modes to the orbital triplet T_{2g} state is less than that to the E_g state. As a consequence, the difference of the coefficient in E_g and $^2T_{2g}$ states produces broad absorption and luminescence bands with large Stokes shift.

Next, consider the Jahn–Teller effect in lower symmetry (tetragonal, trigonal, pseudo-trigonal). The axial crystal field is regarded as a perturbation of the electronic Hamiltonian including the Jahn–Teller effect. The axial field stabilizes or reduces the Jahn–Teller distortion [16]. Figure 7(b) shows a schematic configuration coordinate diagram for Ti^{3+} in pseudo-trigonal symmetry. The lattice coordinates of the horizontal axis are $Q_2(Q_3)$ of the degenerate E_g mode. This configuration coordinate model can explain all the features of the absorption and luminescence of Ti^{3+} in YAB and GAB.

The odd-parity terms in the crystal field expansion are unimportant with respect to level splittings but they are important in allowing electric dipole radiative transitions between the Ti^{3+} levels. Such odd-parity distortions determine both the decay time of luminescence and the polarizations of absorption and emission transitions. The selection rules for the intermanifold transitions of Ti^{3+} ions in sites with octahedral, tetragonal, trigonal and orthorhombic symmetry have been discussed by Yamaga *et al* [16, 17], using a model in which odd-parity distortions mix odd-parity wavefunctions from neighbouring ligand

ions into the even-parity 3d orbitals. They have calculated the transition probabilities between the ^2E excited state and $^2T_2$ ground states induced by $T_{1u}(\sigma)$, $T_{1u}(\pi)$ and $T_{2u}(\pi)$ odd distortions, where σ and π imply that the ligand ions' displacements are parallel and perpendicular to the central-ion–ligand-ion axis, respectively. According to their calculation, the Z-components of $T_{1u}(\sigma)$ and ($T_{1u}(\pi)$, $T_{2u}(\pi)$) in trigonal symmetry produce relative transition probabilities $A_\sigma{:}A_\pi = 2{:}1$ and 1:2, respectively, corresponding to Δ_1^a and Δ_2^a in figure 7 where σ and π mean the electric vector of the radiation is perpendicular to and parallel to the c-axis. The X- and Y-components of $T_{1u}(\sigma)$, $T_{1u}(\pi)$ and $T_{2u}(\pi)$ produce different probabilities, strongly depending on the wavefunctions of the excited state. On the assumption that the probabilities are given by the average of each wavefunction of the excited state, the relative transition probabilities induced by the X (Y) components of $T_{1u}(\sigma)$, $T_{1u}(\pi)$ and $T_{2u}(\pi)$ are $A_\sigma{:}A_\pi = 3{:}1$, 3:4 and 1:0, respectively. The transition probabilities corresponding to Δ_1^e in figure 7, induced by the odd distortions, are the same as those corresponding to Δ_1^a. The probabilities corresponding to Δ_2^a induced by the Z-components of $T_{1u}(\sigma)$, $T_{1u}(\pi)$ and $T_{2u}(\pi)$ are calculated to be $I_\sigma{:}I_\pi = 1{:}0$, 1:0 and 0:0 (forbidden), whereas those induced by their X- (Y-) components are to be $I_\sigma{:}I_\pi = 1{:}8$, 1:2 and 1:4, respectively.

The observed polarization ratios of the absorption are $A_\sigma{:}A_\pi = 1{:}3$ and 1:1.5 for YAB and GAB, respectively, whereas those of the luminescence are 1:1.4 and 1:1.4, respectively. These experimental results indicate that the X-components of $T_{1u}(\pi)$ or the Z-component of $T_{2u}(\pi)$ is dominant. However, it is very difficult to determine which component is more effective from the polarizations of the broad absorption and luminescence bands of Ti^{3+} in YAB and GAB. Although the zero-phonon line gives more detailed information on the energy levels and electronic properties of the $^2T_2$ ground state, it is not observed in YAB and GAB, even at low temperature.

5. Concluding remarks

Interest in the optical properties of Ti^{3+}:YAB and GAB stems from their potential as tunable solid state lasers. The experimental results discussed here show that the absorption and luminescence bands are slightly shifted to longer wavelengths relative to the benchmark system of $Ti^{3+}{:}Al_2O_3$. This follows from the slightly weaker octahedral crystal field term at the Al^{3+} site in these mixed borates compared to the Al^{3+} site in Al_2O_3. ESR studies of Ti^{3+}:YAB reveal the intrinsic presence of odd-parity distortions of the Al^{3+} site in the aluminoborates, which has particular significance for the polarization of the absorption and luminescence spectra. These are discussed in terms of a molecular orbital model of the selection rules for dipole transition of $3d^n$ ions [16, 17], from which it is concluded that it is the Z-component of a $T_{2u}(\pi)$ distortion or X-component of a $T_{1u}(\pi)$ distortion that is particularly important for the polarized optical transition in these crystals.

Acknowledgments

At Strathclyde these researches have been supported by a rolling grant GR/K/04392 jointly funded by EPSRC and the DRA (RSRE). The authors are grateful for the support from the joint research projects between the Japan Society for the Promotion of Science, the British Council and the Royal Society. The authors would like to thank Dr Kindo, Osaka University, for providing the opportunity to measure the ESR spectra at low temperatures.

References

[1] Ballman A A 1962 *Am. Mineral.* **47** 138
[2] Dorozhkin L M, Kuratev I I, Leonyuk N I, Timochenko T I and Shestakov A V 1981 *Sov. Tech. Phys. Lett.* **7** 555
[3] Luo Z D, Lin J T, Jiang A D, Huang Y C and Qui M W 1989 *Proc. SPIE* **1104** 132
[4] Blasse G and Bril A 1967 *Phys. Status Solidi* **20** 551
[5] Kallendonk F, van den Belt T and Blasse G 1982 *J. Chem. Phys.* **76** 1194
[6] Iwai M, Mori Y, Sasaki T, Nakai S, Sarukura N, Liu Z and Segawa Y 1995 *Japan. J. Appl. Phys.* **34** 2238
[7] Wang G, Gallagher H G, Han T P J and Henderson B 1996 *Radiat. Eff. Defects Solids* **136** 953
[8] Wang G, Gallagher H G, Han T P J and Henderson B 1996 *J. Crystal Growth* **163** 272
[9] Wang G, Han T P J, Gallagher H G and Henderson B 1996 *Appl. Phys. Lett.* **67** 3906
[10] Yamaga M, Henderson B, Gao Y, Rasheed F, O'Donnell K P and Cockayne B 1990 *Appl. Phys.* B **51** 329
[11] Gächter B F and Koningstein J A 1974 *J. Chem. Phys.* **60** 2003
[12] Macfarlane R M, Wong J Y and Sturge M D 1968 *Phys. Rev.* **166** 250
[13] Abragam A and Bleaney B 1970 *Electron Paramagnetic Resonance of Transition Ions* (Oxford: Clarendon)
[14] Yamaga M, Yosida T, Henderson B, O'Donnell K P and Date M 1992 *J. Phys.: Condens. Matter* **4** 7285
[15] Yamaga M, Yosida T, Naitoh Y and Kodama N 1994 *J. Phys.: Condens. Matter* **6** 4381
[16] Yamaga M, Henderson B and O'Donnell K P 1991 *Appl. Phys.* B **52** 122
[17] Yamaga M, Henderson B, O'Donnell K P, Rasheed F, Gao Y and Cockayne B 1991 *Appl. Phys.* B **52** 225
[18] Henderson B and Imbusch G F 1989 *Optical Spectroscopy of Inorganic Solids* (Oxford: Oxford University Press) ch 5